Advances in Nonlinear Variational Inequalities
ISSN: 1092-910X
Vol 28 No. 2 (2025)

MHD Non-Uniform Heat Source / Sink for Microorganism Bioconvection Flow on Casson Nanofluid Over an Exponential Stretching Sheet

Avinash B. Raut[1,2], Pradeep G Janthe[1], Jagadish V. Tawade[1*]

[1]Department of Mathematics, Vishwakarma University, Pune, India

[2]Department of Engineering Sciences & Humanities, Vishwakarma Institute of Technology, Pune, India

avinash.raut@vit.edu, pradeepjanthe@gmail.com, jagadish.tawade@vupune.ac.in

* Corresponding author: Jagadish V Tawade (jagadish.tawade@vupune.ac.in)

Article History:

Received: *31-07-2024*

Revised: *20-09-2024*

Accepted: *01-10-2024*

Abstract:

This study explores the numerical analysis of Casson nanofluid flow over an exponential stretching sheet, incorporating the effects of magnetic field, nonuniform heat source/sink, activation energy and motile microorganisms. The primary aim of the current study is to investigate the effects of these factors on the bioconvection dynamics within the fluid. By using a bvp4c algorithm, the governing equations that describe the nanofluid flow, taking into account of the non-Newtonian Casson fluid behaviour over an exponential stretching sheet's velocity, temperature and concentration profiles along with the influence of activation energy on chemical reactions. Additionally, the study examines how motile microorganisms interact with the nanofluid flows, affecting the bioconvection patterns and overall fluid behaviour. The analysis provides a comprehensive understanding of the interplay between these variables and their effect on heat and mass transfer in the system. The results reveal that, for higher activation energy increases the temperature gradient and concentration fields, affecting the overall bioconvection process. The motile microorganisms impact to the bioconvection process by affecting the concentration and velocity fields. Their presence modifies the bioconvection patterns, which can either enhance or suppress the convective transport depending on their density and motility. Also, an increase in the values $A*$ and $B*$ leads to a enhance the fluid temperature.

Keywords: MHD, Nonuniform Heat source/sink, activation energy; bioconvection; Casson nanofluid; exponential stretching sheet; motile microorganism.

1.Introduction:

The combined heat and mass transfer problems for nanofluids are important in many processes and have moved a lot of attention among the researchers in recent years. A fluid that contains nanoparticles-tiny particles with a diameter measured in nanometers-is referred to as nanofluid. Metals, oxides, and carbides can all be used to create these nanoparticles. Nano fluids obtain by suspending such nano particles in the base fluid.

Lone et al. (1,2) investigated the computational analysis of MHD-driven bioconvective flow of hybrid Casson nanofluid past a permeable exponential stretching sheet with thermophoresis and Brownian

motion effects, as well as the stratified flow of a non-Newtonian Casson fluid containing microorganisms on a stretching sheet with activation energy. Homotopy study on the bio-inspired radiative magnesium and iron oxides/blood nanofluid flow over an exponential stretching sheet was studied by Jayavel et al. (3). Activation energy and variable thermal conductivity were investigated by Mondal et al. (4) in relation to a magneto-convective nonlinear thermo-radiative Casson nanofluid containing motile microorganisms across a sinusoidal surface. The activity of motile microorganisms in bioconvective nanofluid flow with Arrhenius activation energy was discussed by Mandal et al. (5). The Stagnation Point Flow of Casson Nanofluid with Thermal Radiation and Swimming Microorganisms over a Stretching Sheet: A Computational Modelling via Analytical Method was explored by Sekhar et al. (6). The Homotopic modelling of MHD bioconvective flow of a water-based hybrid nanofluid over a thermal convective exponential stretching surface was investigated by Shamshuddin et al. (7). In the study of Waqas et al. (8) the effects of activation energy and an exponential heat source/sink on the bioconvectional flow of burger nanofluid over an inclined wall beneath swimming microorganisms was discussed. Basit et al. (9) explored the numerical simulation of a bioconvective Casson nanofluid over an exponentially permeable stretched surface. Using gyrotactic microorganisms and activation energy, Ahmad et al. (10) explored the thermally generated Cattaneo-Christov Maxwell nanofluid over a bidirectional periodically accelerated surface. The bioconvective treatment of reactive Casson hybrid nanofluid flow via an exponentially stretched sheet using mixed convection and ohmic heating was elaborated by Shamshuddin et al. (11). Makkar et al. (12) investigated the three-dimensional modelling of magnetohydrodynamic bio-convective Casson nanofluid flow with buoyancy effects whereas Khan et al. (13) investigated the bioconvection Maxwell nanofluid flow across a stretching cylinder with activation energy. By using motile microorganisms, Imran et al. (14) investigated the physical characteristics of bio-convection in nanofluid flow through a paraboloid of revolution on a horizontal surface. Khan et al. (15) investigated the Sisko nanofluid's natural bio-convective flow in response to activation energy and gyrotactic microorganisms.

The magnetohydrodynamic stretched flow of Williamson Maxwell nanofluid via a porous matrix over a penetrated sheet was investigated by Sohaib et al (16). The bioconvection of MHD second-grade fluid transporting nanoparticles over an exponentially extending sheet: An application for biofuel was investigated by Siddique et al. (17). The Cattaneo-Christov heat diffusion on MHD Casson-Williamson bioconvective nanofluid flow across an exponential porous stretched sheet was analysed by Patil et al. (18). The effects of thermophoresis and Brownian motion on radiative MHD hybrid nanofluid flow across a stretching sheet with convective boundary conditions were studied by Hussain et al. (19) using a homotopic approach.

In the study of Habib et al. (20) the function of activation energy and bioconvection in time-dependent nanofluid slip transpiration caused by domain extension in the presence of electric and magnetic fields was discussed. The thermo-bioconvective flow of a 3D rotating Williamson nanofluid with an Arrhenius activation energy in a Darcy-Forchheimer medium over an exponentially extending surface was studied by Bafe et al. (21). The Homotopic analysis for bioconvection of Casson nanofluid flow across an exponential stretching sheet with activation energy and motile microbe was investigated by Sankari et al. (22).

This work distinguishes from the available literature that it is an unique contribution in the domain of current research. The main investigation is found in the thorough analysis of the combined effects of several parameters, including the thermal radiation, buoyancy forces, magnetic field, activation energy, permeability of porous media, thermophoresis, non-uniform heat source/sink, and Brownian motion. These complex interactions are investigated in the setting of bioconvection, where a permeable nonlinear stretching sheet passed by a reactive nanofluid made up of motile bacteria. The bvp4c method is used to solve by highly nonlinear ordinary differential equations. Through graphics, the physical effects of velocity, thermal and concentration flow profiles are presented in this study.

Nomenclature	
B_0 − Strength of magnetic field	T − Temperature (K)
C_∞ − Ambient concentration (kg/m^3)	T_∞ − Ambient temperature (K)
C_P − Specific heat (J/kgK)	x, y − coordinates (m)
T_w − Temperature near the surface (K)	μ − Dynamic velocity (Kgm^2/s)
u, v − Velocity components (m/s)	U_w −Stretching velocity (m/s)
ν − Kinematic viscosity(m^2/s)	ρ − Fluid density (kg/m^3)
k − Thermal conductivity $(W/m/K)$	D_T −Thermophoretic diffusion coefficient (m^2/s)
U_∞ −Free stream velocity	
V_w − Suction/injection velocity (m/s)	D_m −Microorganismdiffusionconstant(m^2/s)
g − Acceleration due to gravity (m/s^2)	D_B −Brownian diffusion coefficient (m^2/s)
Kr − Chemical reaction rate constant	σ − Electrical conductivity
α − Thermal diffusivity (m^2/s)	f − Dimensionless stream function
ψ − Stream function (m^2/s)	ϕ − dimensionless concentration
θ − Dimensionless temperature	**Subscripts**
C − Fluid concentration (kg/m^3)	w −Condition at the surface
C_s − Concentration near the surface(kg/m^3)	∞ −Condition at free stream

2. Mathematical formulation

To demarcate the primary equations governing the current flow issue, the subsequent assumptions have been made. Figure 1 delineates the tangible facets of the issue. The analysis context assumes a two-dimensional boundary stratum drift of a viscous, incompressible liquid. The boundary stratum is assumed to be electrically conductive. A magnetic field of uniform strength B_0 is applied to the plate surface in the positive y-axis direction. The membrane within the permeable medium is assumed to expand exponentially. Heat and mass exchange phenomena are assumed to include Brownian and thermophoresis dispersals. The equation is adapted to include a thermal source and integrate thermal radiation mechanisms. Ohmic dispersion and joule heating are assumed to affect the energy equation. Activation energy is assumed to have a significant impact on the migration process. The interplay between nanofluid composition and gyrotactic mobile microorganisms is assumed to be relevant.

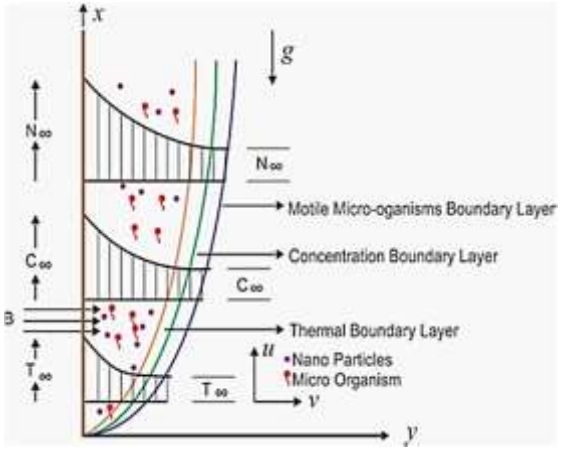

Figure 1. The schematic diagram of the flow problem

It is presumed that the exterior is being extended along the x-axis with velocity $U(x)$ and that the y-axis is parallel. Temperature variance is created by preserving the exterior at a temperature $T_w(x)$ higher than the $T_\infty(x)$ surrounding fluids (constant temperature) and maintaining a concentration $C_w(x)$ more significant than the surrounding fluids $C_w(x)$ (constant concentration). There is an assumption that $T_\infty(x) = T_0 + ce^{x/2L}, T_w(x) = T_0 + be^{x/2L}, C_\infty(x) = C_0 + ne^{x/2L}, C_w(x) = C_0 + me^{x/2L}$ where is T_0 the position temperature, C_0 is the position concentration, and $b, c, m,$ and n are optimistic and persistent. The governing equations for liquid transport are

$$\frac{\partial u}{\partial x} + \frac{\partial v}{\partial y} = 0 \tag{1}$$

$$u\frac{\partial u}{\partial x} + v\frac{\partial v}{\partial y} = v\left(1 + \frac{1}{\beta}\right)\frac{\partial^2 u}{\partial y^2} - \frac{\sigma B_0^2 u}{\rho} - \frac{v}{k'}u \tag{2}$$

$$+\frac{1}{\rho}\left[g\beta\rho(1 - C_\infty)(T - T_\infty) - g\left(\rho_P - \rho_f\right)(C - C_\infty) - gy\left(\rho_m - \rho_f\right)(N - N_\infty)\right]$$

$$u\frac{\partial T}{\partial x} + v\frac{\partial T}{\partial y} = \alpha\frac{\partial^2 T}{\partial y^2} - \frac{1}{\rho C_p}\frac{\partial q_r}{\partial y} + \frac{\vartheta}{C_p}\left(\frac{\partial u}{\partial y}\right)^2 + \frac{\sigma B_0^2 u^2}{\rho C_p} + \vartheta\frac{u^2}{k'C_p} \tag{3}$$

$$+\tau\left[D_B\frac{\partial C}{\partial y}\frac{\partial T}{\partial y} + \frac{D_T}{T_\infty}\left(\frac{\partial T}{\partial y}\right)^2\right] + \frac{q'''}{\rho C_p}$$

$$u\frac{\partial C}{\partial x} + v\frac{\partial C}{\partial y} = D_B\frac{\partial^2 C}{\partial y^2} - \frac{D_T}{T_\infty}\frac{\partial^2 T}{\partial y^2} - \mathrm{K}_r^2(C - C_\infty)\left(\frac{\mathrm{T}}{T_\infty}\right)^n \exp\left(\frac{-Ea}{kT}\right) \tag{4}$$

$$u_a\frac{\partial N}{\partial x} + v_b\frac{\partial N}{\partial y} + bW_c\frac{\partial}{\partial y}\left(\frac{n}{\Delta C}\frac{\partial C}{\partial y}\right) = D_m\frac{\partial}{\partial \mathrm{y}}\frac{\partial N}{\partial \mathrm{y}} \tag{5}$$

The rate components u and v correspond to the liquid's motion in the x and y orders, while T signifies the temperature of the liquid, and the permeability is $k' = K^* e^{-x/L}$ where K^* is insistent.

The system represents $k_r = \frac{1}{2}\left(\frac{k_0}{m}\right)e^{x/2L}$ the inconstant chemical change rate in a second-order irrevocable reaction and k_0 is a constant. Following the Roseland

approximation for the radiative heat flux $\frac{\partial q_r}{\partial y} \approx \frac{-16\sigma^* T_\infty^3}{3k^*}\frac{\partial^2 T}{\partial y^2}$ where k^* is the mean absorption coefficient and σ^* is Stefan-Boltzmann constant. The equivalent boundary restrictions are:

$$u = U = U_0 e^{x/2L}, v = -V(x) = -V_0 e^{x/L}, T = T_w(x) = T_0 + be^{x/2L},$$
$$C = C_w(x) = C_0 + me^{x/2L}, \qquad N = N_w(x) = N_0 + pe^{x/2L}, at\ y = 0. \qquad (6)$$
$$u \to 0, T = T_\infty(x) = T_0 + ce^{x/2L}, C = C_\infty(x) = C_0 + ne^{x/2L},$$
$$N = N_\infty(x) = N_0 + qe^{x/2L}\ at\ y \to \infty. \qquad (7)$$

Here, Reference velocity is denoted by U_0 suction velocity by $V(x) > 0$ and blowing velocity by $V(x) < 0$. The initial suction strength is symbolized by $V_0 > 0$, and the initial blowing strength is represented by $V_0 < 0$.

Similarity variables:

$$\eta = \sqrt{\frac{U_0}{2\vartheta L}}e^{x/2L}y, \qquad u = U_0 e^{x/L} f'(\eta), \qquad v = -\sqrt{\frac{\vartheta U_0}{2L}}\ e^{x/2L}\{f(\eta) + \eta f'(\eta)\}$$
$$\theta(\eta) = \frac{\mathrm{T} - T_\infty}{T_W - T_\infty}, \qquad \phi(\eta) = \frac{\mathrm{C} - C_\infty}{C_W - C_\infty}, \qquad \chi(\eta) = \frac{\mathrm{N} - N_\infty}{N_W - N_\infty} \qquad (8)$$

Heat source (> 0) or sink (< 0) per unit volume is represented as

$$q''' = \frac{kU}{2L\vartheta}[A^*(T_w - T_0) + B^*(T - T_0)]$$

By applying the similarity transformation described above, Eq. (1) is trivially satisfied, and Eqs. (2)–(8) become:

$$\left(1 + \frac{1}{\beta}\right)f''' + ff'' - 2f'^2 - Mf' - Kpf' + \omega(\theta - Nr\phi - Rb\chi) = 0 \qquad (9)$$

$$\left(1 + \frac{4}{3}R\right)\theta'' + \mathrm{Pr}\left(f\theta' - f'\theta - \mathrm{Ts}\,f' + Nb\phi'\theta' + \mathrm{Nt}(\theta')^2\right)$$
$$+ \mathrm{Pr}\,Ecf''^2 + Pr\ Ec\ Kp\ f'^2 + [A^*f' + B^*\theta] = 0 \qquad (10)$$

$$\phi'' + Sc\left(f\phi' - f'\phi - Csf' - A\phi(1 + \delta\theta)^m\ exp\left(\frac{-E}{1 + \delta\theta}\right)\right) + \frac{Nt}{Nb}\theta'' = 0 \qquad (11)$$

$$\chi'' + Sb(\chi' f - \chi f) - Sb\ Ms\ f' - Pe[\phi''(\chi + \Omega) + \chi'\phi'] = 0 \qquad (12)$$

The corresponding boundary conditions are

$$f = S, f' = 1, \theta = 1 - \mathrm{Ts}, \phi = 1 - \mathrm{Cs}, \chi = 1 - \mathrm{Ms}, \text{at } \eta \to 0$$
$$f' \to 0, \theta \to 0, \phi \to 0, \chi \to 0, as\ \eta \to \infty. \qquad (13)$$

Wherever the prime symbolizes differentiation concerning η, $Kp = \frac{2L\vartheta}{K^* U_0}$ is porous stricture,

$M = \frac{2L\sigma B_0^2}{\rho U_0 e^{x/L}}$ means magnetic stricture, $Pr = \frac{\vartheta}{\alpha}$ a is the Prandtl number, $Ts = \frac{c}{b}$ is the thermally stratified stricture, $Sc = \frac{\vartheta}{D}$ denotes the Schmidt number, $Cs = \frac{n}{m}$ is chemically stratified stricture, $S = \frac{V_0}{\sqrt{\frac{\vartheta U_0}{2L}}}$ is the suction or blowing stricture. S > 0 denotes the suction constraint, while S < 0 represents the blowing constraint, Ms denotes the motile density stratified structure, and the mixed convection constraint is signified as $\omega = \frac{(1-C_\infty)\beta g(T_W-T_\infty)2L}{U_0^2 e^{2x/L}}$. The buoyancy ratio number is meant as $Nr = \frac{(\rho_p-\rho_f)(T_W-T_\infty)}{(1-C_\infty)\beta\rho(T_W-T_\infty)}$. The bioconvection Rayleigh number is represented as $Rb = \frac{(\rho_m-\rho_f)\gamma(N_W-N_\infty)}{(1-C_\infty)\beta\rho(T_W-T_\infty)}$. The Brownian factor is indicated by $Nb = \frac{\tau D_B(C_W-C_\infty)}{\vartheta}$. The thermophoresis diffusion aspect is characterized as $Nt = \frac{\tau D_T(T_W-T_\infty)}{\vartheta T_\infty}$. The radiation restriction is symbolized as $R = \frac{4\sigma * T_\infty^3}{k^* K}$. The bioconvection Schmidt number is designated as $Sb = \frac{\vartheta}{D_m}$. $Ec = \frac{U_0^2}{Cp}\frac{e^{2x/L}}{(T_W-T_\infty)}$ is the Eckert Number.

The Peclet number is signified as $Pe = \frac{bW_n}{D_n}$. The non-dimensional energy activation is symbolized as $E = \frac{E_a}{kT_\infty}$. The dimensionless reaction rate is symbolized as $A = \frac{2k_r^2 L}{U_0}$. The essential physical quantities of interest are the drag force factor$Cf_x = \frac{\tau_w}{\rho U^2/2}$, local Nusselt number $Nu_x = \frac{xq_w}{k(T_W-T_\infty)}$, local Sherwood number $Sh_x = \frac{xq_n}{D_m(N_W-N_\infty)}$Shx ¼ xJw DðCw−C1Þ , and Motile density number $Nn_x = \frac{xJ_w}{D(C_W-C_\infty)}$ where $\tau_w, q_w, and\ J_w$ are the shear stress, heat flux, and mass flux at the surface,

$$\tau_w = \mu\left(\frac{\partial u}{\partial y}\right)_{y=0}, q_w = -k\left(1+\frac{4R}{3}\right)\left(\frac{\partial T}{\partial y}\right)_{y=0}, \qquad and\ J_w = -D\left(\frac{\partial C}{\partial y}\right)_{y=0},$$
$$q_n = -D_m\left(\frac{\partial N}{\partial y}\right)_{y=0} \tag{14}$$

Employing Eq. (7), the non-dimensional drag force coefficient, as well as the rates of wall heat and mass transference, are determined:

$$f''(0) = \frac{C_f}{\sqrt{\frac{2}{Re}}\sqrt{\frac{x}{L}}}, -\left(1+\frac{4R}{3}\right)\theta'(0) = \frac{Nu(1-Ts)}{\sqrt{\frac{2}{Re}}\sqrt{\frac{x}{L}}},$$
$$\text{and } -\phi'(0) = \frac{Sh(1-Cs)}{\sqrt{\frac{2}{Re}}\sqrt{\frac{x}{L}}}, -\chi'(0) = \frac{Nn(1-Ms)}{\sqrt{\frac{2}{Re}}\sqrt{\frac{x}{L}}} \tag{15}$$

The local Reynolds number is designated by $Re = \frac{Ux}{\vartheta}$

3. Numerical Solution:

The model (14) – (17) consists of highly non-linear coupled ordinary differential equations. Exact solutions of the same are not possible. Literature survey suggests that such equations are solved either numerically or by using bvp4c. In the present case we adopt the efficient bvp4c method to obtain the numerical solutions of (14)–(17). The coupled ordinary differential equations (14) and (15) are reduced to a set of simultaneous first order equations as follows.

$$\left.\begin{array}{c} f = y_1, f' = y_2, f'' = y_3, \\ \theta = y_4, \theta' = y_5, \\ \phi = y_6, \phi' = y_7, \\ \chi = y_8, \chi' = y_9 \end{array}\right\} \quad (16)$$

$$f''' = \left(\frac{-1}{1+\frac{1}{\beta}}\right)[y_1 y_3 - 2{y_2}^2 - My_2 - Kpy_2 + \omega(y_4 - Nry_6 - Rby_8)] \quad (17)$$

$$\theta'' = \left(\frac{-1}{1+\frac{4}{3}R}\right)[Pr(y_1 y_5 - y_2 y_4 - Tsy_2 + Nby_7 y_5 + Nt(y_5)^2) + PrEc(y_3)^2$$

$$+PrEcKp(y_2)^2 + [A^* y_2 + B^* y_4]] \quad (18)$$

$$\phi'' = -\left[Sc\left\{y_1 y_7 - y_2 y_6 - Csy_2 - Ay_6(1+\delta y_4)^m . exp\left(\frac{-E}{1+\delta y_4}\right)\right\} + \frac{Nt}{Nb}\theta''\right] \quad (19)$$

$$\chi'' = -[Sb(y_9 y_1 - y_8 y_1) - SbMsy_1 - Pe\{\phi''(y_8 + \Omega) + y_7 y_9\}] \quad (20)$$

Corresponding boundary conditions take the form,

$$y_1 = S, y_2 = 1, y_4 = 1 - Ts, y_6 = 1 - Cs, y_8 = 1 - Ms \quad \text{at } \eta = 0$$

$$y_2 = 0, y_4 = 0, y_6 = 0, y_8 = 0 \text{ at } \eta \to \infty. \quad (21)$$

4. Results and discussion:

This section presents the simulation results for the transient three-dimensional magnetohydrodynamic flow of a Casson nanofluid past a stretching sheet with non-uniform heat source/sink, thermal radiation, and chemical reaction. Notably, the Casson fluid parameter exhibits anisotropic behaviour, increasing in the x-direction and decreasing in the y-direction, while the magnetic parameter decreases in both directions. The heat and mass transfer rates are enhanced with increasing Casson and magnetic field parameters. Furthermore, the chemical reaction parameter modulates the surface skin friction, increasing it in the x-direction and decreasing it in the y-direction. The Nusselt and Sherwood numbers are significantly influenced by parameter variations, with increasing Prandtl number elevating the local Nusselt number and decreasing the Sherwood number, as shown in through graphs.

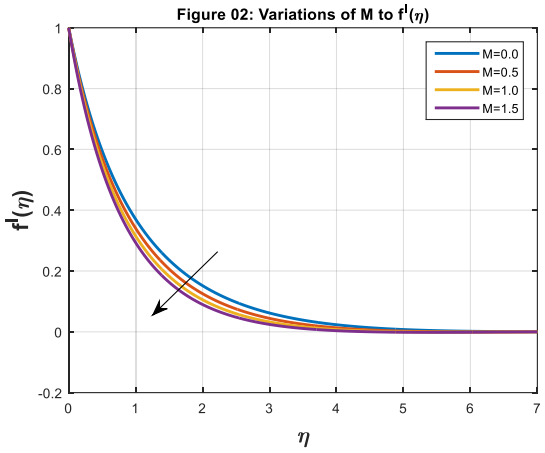

Figure 2 shows how the magnetic field affects It demonstrates that when the magnetic field intensity is increased, the overall velocity gradient decreases and the velocity near the extending sheet increases as a result of an accelerating electric field. As an obstructive force, the Lorentz force increases the frictional resistance that resists the drive of nanofluid inside the thickness of the momentum barrier stratum. As a consequence, this causes the nano-liquid velocity profile outside to increase in size.

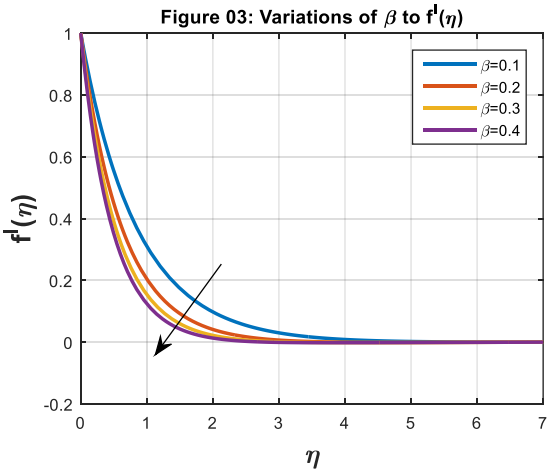

The effect of the Casson liquid stricture b on a liquid's velocity gradient is seen in Figure 3. The figure shows that when the Casson liquid constraint (b) increases, the fluid velocity falls and the fluid viscosity rises. This behaviour is explained by the fact that the yield stress, which impedes fluid motion inside the fluid layer close to the boundary, causes an increase in viscosity. The Casson constraint on velocity gradients was motivated by the way it describes the rheological properties of fluids under yield stress. In particular, the Casson parameter controls these fluids' shift from viscous to plastic behaviour.

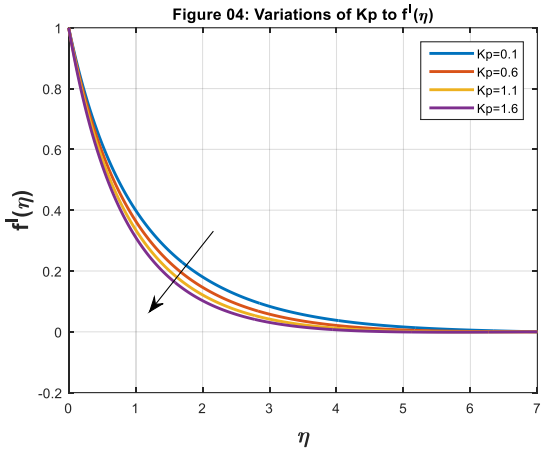

The effect of the porosity limit on velocity is illustrated in Figure 4. It is shown that porosity impact causes an increase in fluid resistance and a decrease in fluid velocity, which in turn results in the damping qualities of fluid take-up. A porous material restricts fluid flow more severely, delaying the fluid's movement and raising surface shear stress as a result. Therefore, when the permeability stricture upsurges, so does the barrier to liquid motion. The liquid's velocity decreases as a result.

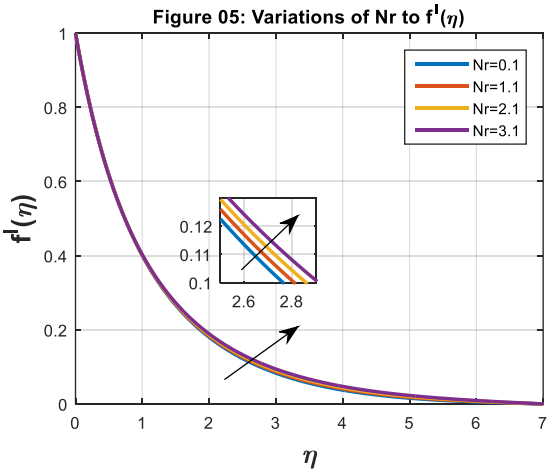

Figure 5 looks into the relationship between velocity and the buoyancy ratio structure. This figure shows that when the buoyancy ratio stricture decreases, the velocity increases. The importance of buoyant forces in relation to inertial forces is captured by the buoyancy ratio parameter. When the buoyancy ratio is high, the flow behaviour is dominated by the buoyancy forces. Under such conditions, density differences brought on by temperature gradients are the main force behind fluid motion.

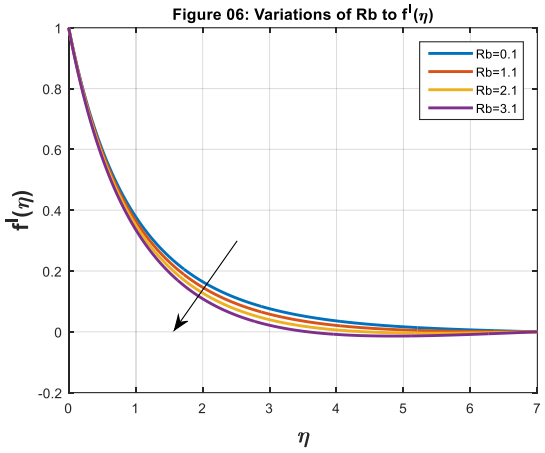

The relationship between velocity and Rb is seen in Figure 6. The figure suggests that the velocity gradient decreases as the bioconvection Rayleigh number increases. This pattern suggests that in bioconvection, Rb and velocity have an inverse relationship. This Rayleigh number combines the effects of viscosity and buoyancy. The greater Rayleigh number indicates the dominance of buoyant forces over viscous forces. This frequency causes buoyancy-driven convection to drive more intense fluid motion, which boosts energy.

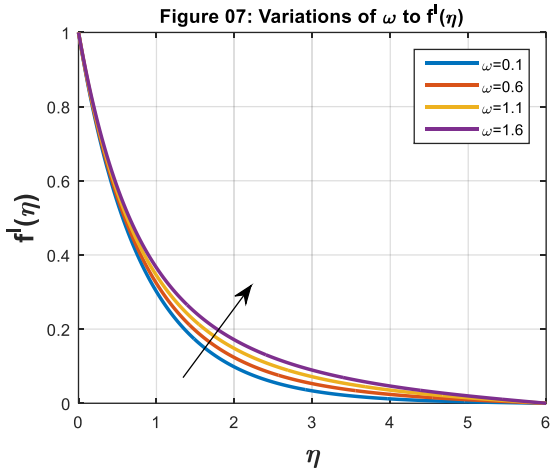

The purpose of Figure 7 is to highlight the important elements of the mixed convection speed constraint. For both surfaces, it is seen that the velocity exhibits larger fluctuations as the magnitude of w increases. This increased velocity fluctuation is particularly apparent in the flat plate configuration. Practically speaking, the mixed convection constraint clarifies the relationship between viscous and inertial forces. Higher levels of this coefficient lead to stronger inertial forces, which in turn raise the liquid's velocity.

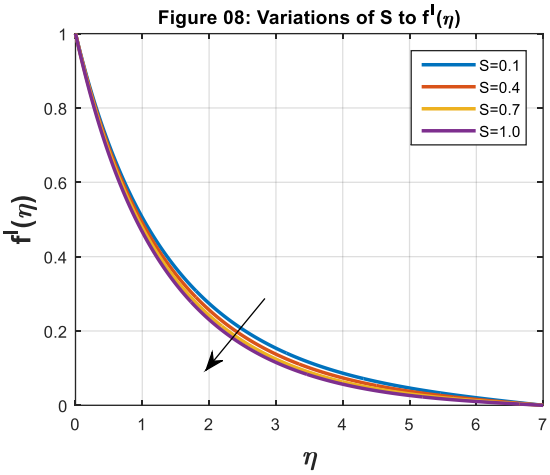

The suction stricture on the velocity gradient for an exponentially growing sheet is inspired by what is seen in Figure 8. The interaction between the boundary stratum close to the stretched sheet and the external flow provides a physical explanation for these phenomena. The boundary layer is efficiently evacuated by suction, which thins it and lowers its velocity. In contrast, blowing encourages the heated fluid to travel outward from the wall, where viscosity has less of an impact, causing the fluid to accelerate and gain velocity.

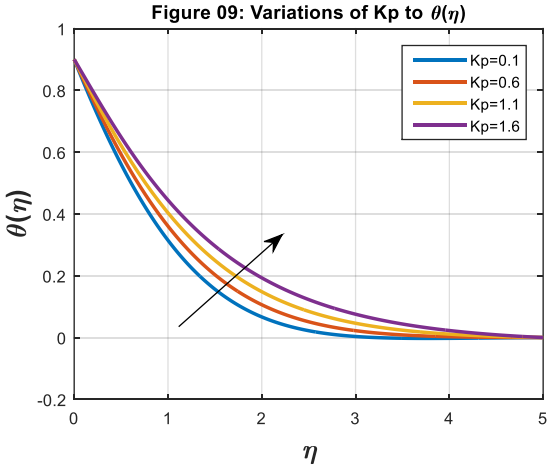

The effect of the porosity constraint on the temperature gradient is illustrated in Figure 9. The porosity parameter regulates several parameters in porous medium, which is the source of its influence on temperature gradients. These variables include fluid velocity, surface area for heat exchange, thermal conductivity, fluid flow, and heat transfer processes. For the purpose of accurately forecasting and controlling temperature gradients in porous materials and their various applications, a thorough grasp of how porosity affects these factors is essential.

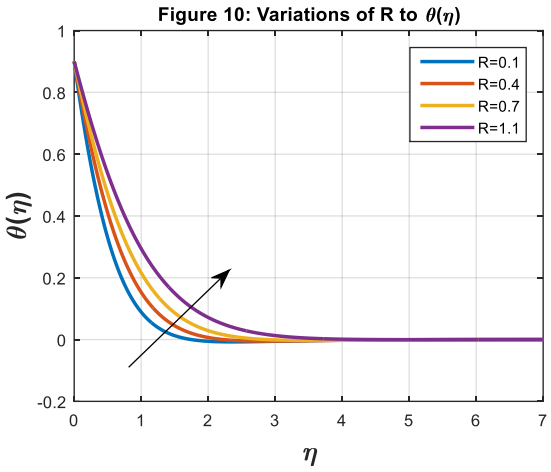

The effect of the thermal radiation constraint on the temperature field is shown in Figure 10. The figure shows how thermal radiation causes the system's temperature to rise. This is due to the fact that thermal radiation raises the fluid's temperature by adding more heat to it. One way that heat can be transferred by electromagnetic waves is through thermal radiation, which can improve energy exchange within the system. Because thermal radiation transfers heat energy through electromagnetic waves emitted by objects, temperature gradients arise within the system. The system's temperature varies as a result of this occurrence.

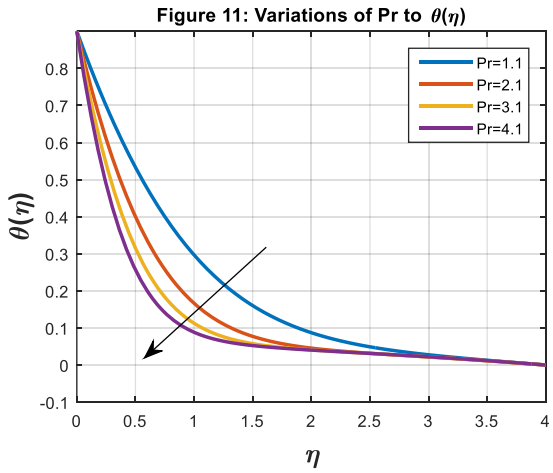

The impact of Pr on temperature gradient is seen in Figure 11. The graph shows that Pr causes the temperature gradient to decrease. The opposing relationship between Pr and thermal diffusivity is what causes this tendency. As the temperature concentration rises, Pr falls. Thermal diffusion and the Prandtl stricture behave differently physically. Consequently, a fluid that has a higher Prandtl number disperses more slowly than one that has a lower Prandtl number. As a result, species' radiation fields become smaller.

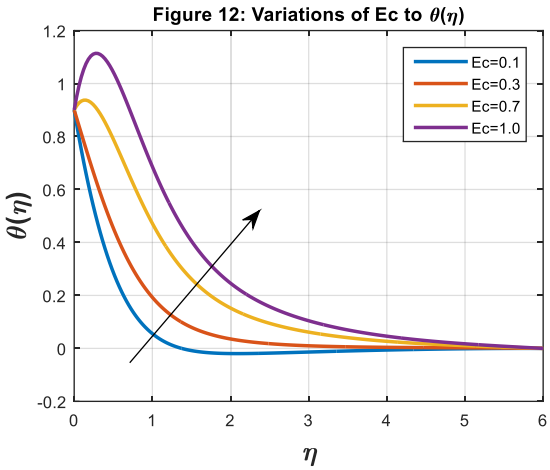

As seen in Figure 12, frictional forces cause thermal energy to become trapped in the liquid when the Eckert number rises. An enhanced temperature distribution results from this. The faster conversion of nano thermal energy due to the enhanced kinetic energy encourages heat retention and redistribution within the fluid. The Eckert number on temperature gradients was inspired by the way it represents the formation of thermal energy and the dissipation of kinetic energy in the fluid flow. The way thermal energy and temperature gradients are distributed throughout the system is directly affected by this characterisation.

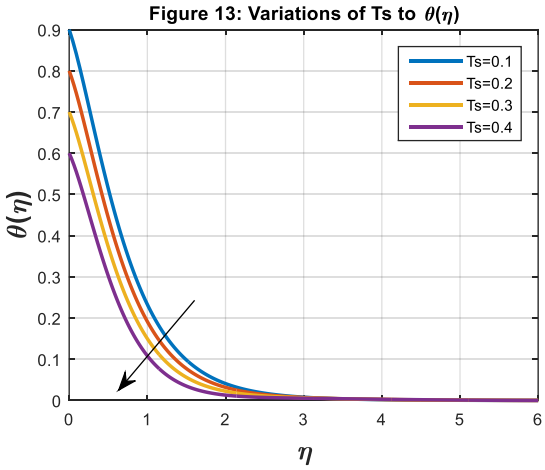

The influence of thermal stratification on temperature is seen in Figure 13. The graphic shows that when the stricture St grows, the temperature decreases. This pattern illustrates how the temperature gradient inspires thermal stratification. Heat transmission processes within the fluid are impacted by the temperature gradient caused by thermal stratification. Thermal energy automatically shifts the gradient itself and the distribution of temperatures by moving from warmer to colder areas. The fluid's thermal composition is greatly shaped by this essential heat transmission process.

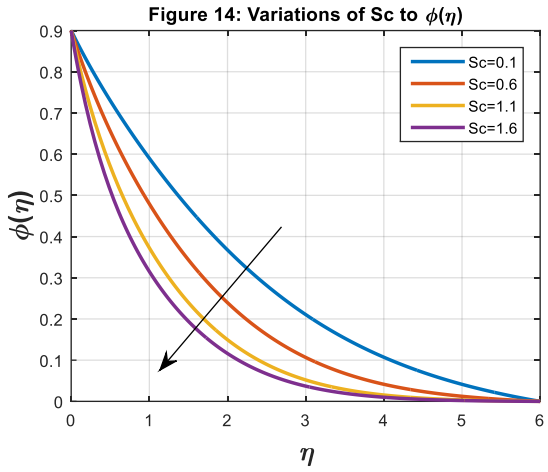

The inspiration behind various Sc values on the concentration distribution is seen in Figure 14. Based on the observations presented in the Figure, it appears that the concentration decreases as Sc increases. The mass diffusivity, which is inversely proportional to the Schmidt number, is connected to this behaviour. A thinner concentration boundary layer results from the decrease in mass diffusivity that is linked to a rise in Sc. As a result of less effective mass transfer and longer diffusion times across the boundary stratum, the concentration profile close to the exterior is reduced.

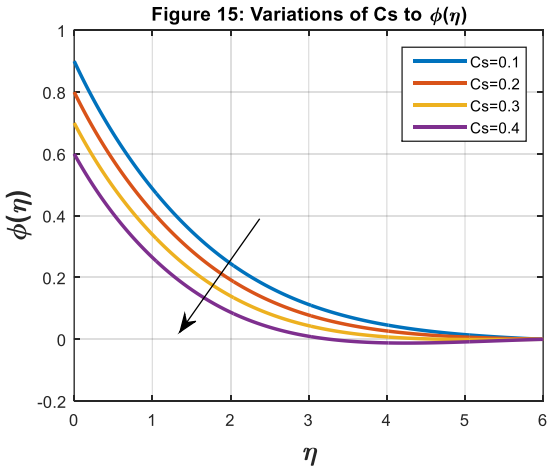

The influence of solutal stratification Cs on concentration is seen in Figure 15. The figure illustrates how the concentration falls with increasing parameter Cs. The liquid near the surface and the top plate have different concentrations as a result of this higher stratification. As a result of the system's increased barrier to solute transfer brought on by solutal stratification, the concentration falls overall. The average concentration decreases as a result of the denser, more concentrated layers close to the surface preventing solute mixing.

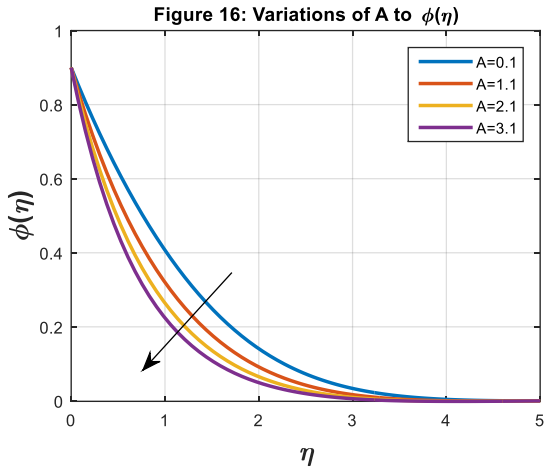

Figure 16 exposes the inspiration of a chemical reaction on fluid concentration. The concentration curves rose as a result of the chemical reaction's steadily rising values. A solution with higher solute concentrations experiences more collisions over time, which accelerates the process. Examining the interplay between reactant and product concentration variations, mass transport processes including diffusion, and reaction kinetics is necessary to comprehend the basic physical laws guiding how chemical reactions affect concentration gradients. For accurate modelling and prediction of the behaviour of chemical systems and their concentration gradients, mastery of these dynamics is essential.

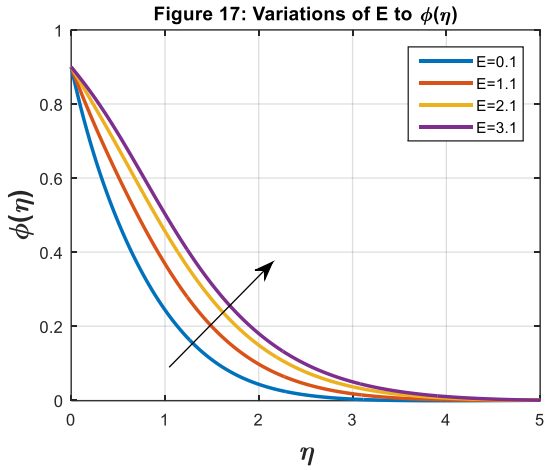

The impact of E on the concentration distribution is indicated in Figure 17. The concentration gradient appears to advance as the non-dimensional activation energy stricture E becomes more intense, as depicted in the figure. Based on this behaviour, it can be concluded that greater activation energy values speed up the chemical process and enhance mass transfer or concentration. Activation energy affects concentration gradients because it is involved in regulating reaction rates, equilibrium behaviour, temperature sensitivity, and reactant and product dispersion in space within chemical systems. Comprehending these phenomena is essential to predicting and controlling concentration gradients in a variety of chemical reactions.

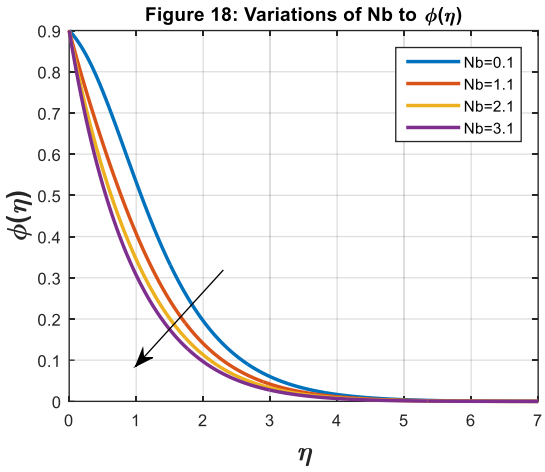

The relationship between the Brownian motion stricture Nb is shown in Figure 18. Increased thermal diffusion is caused by the frequent arbitrary mobility of nanoparticles in the boundary layer, which is indicated by higher levels of Nb. A thorough comprehension of Brownian motion's impacts is necessary to accurately forecast concentration gradients in systems that are affected by it. In order to shape concentration gradients, Brownian motion is essential for encouraging diffusion, creating equilibrium concentrations, improving mixing, enabling particle movement, and spreading particles within the fluid.

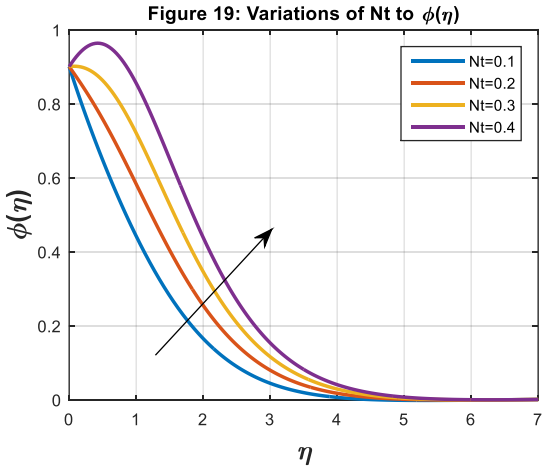

As the thermophoretic measure rises, Figure 19 illustrates how the mass transference rate decreases. The concentration decreases as a result of the nanoparticles moving around more as the temperature gradient increases. Mass moves more slowly as the thermophoretic parameter is increased because the temperature variations become more noticeable. Because thermophoresis can cause particle displacement in response to temperature gradients, it has an impact on concentration gradients. This causes localised changes in the concentration of particles, which in turn affects the concentration gradients in the fluid.

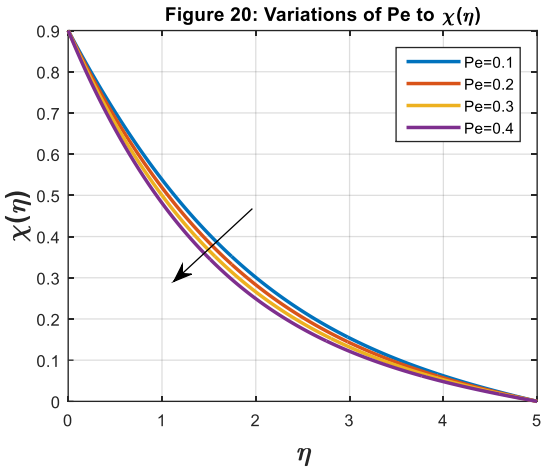

The purpose of Figure 20 is to show how Pe becomes inspired on the gradient of motile microorganisms. This figure illustrates how the diffusion coefficient and microbe density profile rise with increasing Pe over the border stratum's whole thickness. It explains how the components of the fluid move. It is found that when the Peclet number rises, microbial diffusivity increases. The density of motile microorganisms is increased by the physical increase in cell propulsion speed caused by the Peclet number. when a result, bacteria become more mobile and diffusible when Pe values rise.

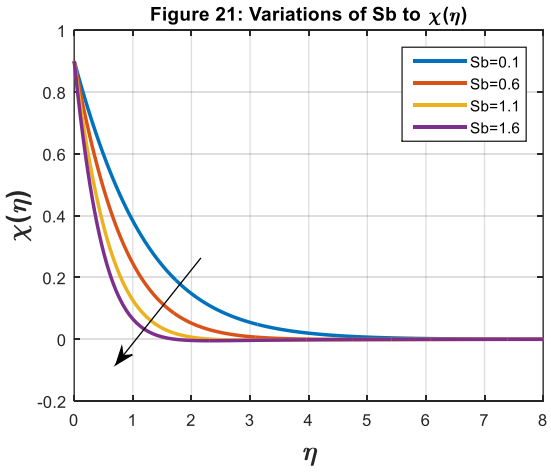

The origin of the bioconvection Schmidt number on the motility field $\chi(\eta)$ is shown in Figure 21. According to the figure, liquid motility decreases as the bioconvection Schmidt number increases. The Schmidt constraint on bioconvection assesses the relative significance of advection vs diffusion in the movement of microorganisms in a fluid medium. It is computed as the product of fluid kinematic viscosity and microorganism diffusivity. Diffusion dominance is indicated by a greater bioconvection Schmidt value, which means that microorganisms diffuse more readily than they move with fluid flow, creating noticeable bioconvetion structures.

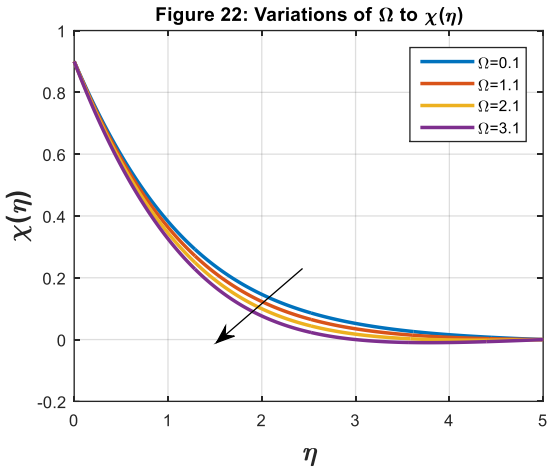

The relationship between the liquid motile density and the concentration difference constraint on microorganisms is examined in Figure 22. The figure shows that at large values of X, the liquid's motile density decreases. It is hypothesised that the concentration difference stricture has a significant impact, increasing the concentration of mobile organisms close to the ambient border stratum.

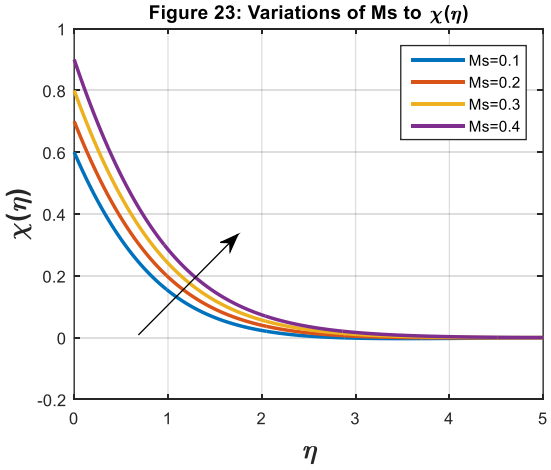

The effect of microbial stratification on the microorganism density profile is seen in Figure 23. Physically, the liquid near the exterior appears to have a lower microbe density than the surrounding liquid, according to the figure. This indicates that the microorganisms are arranged in layers within the liquid. The complex relationship between microorganism gradients and stratification of microorganisms arises from the complex interplay of microbe behaviour, habitat preferences, metabolic activity, interactions with other organisms, and environmental adaption. Together, these elements influence how bacteria are distributed vertically in the fluid, which helps to create gradients of microorganisms.

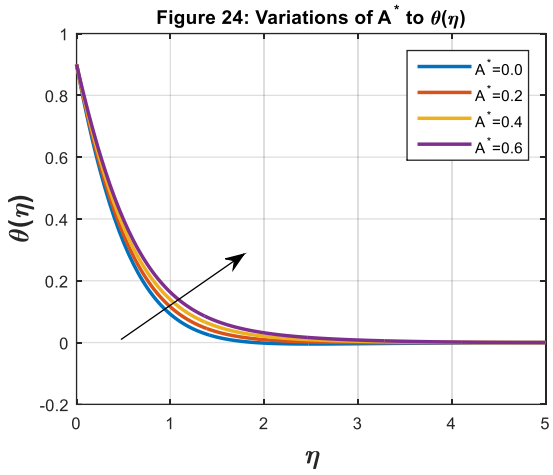

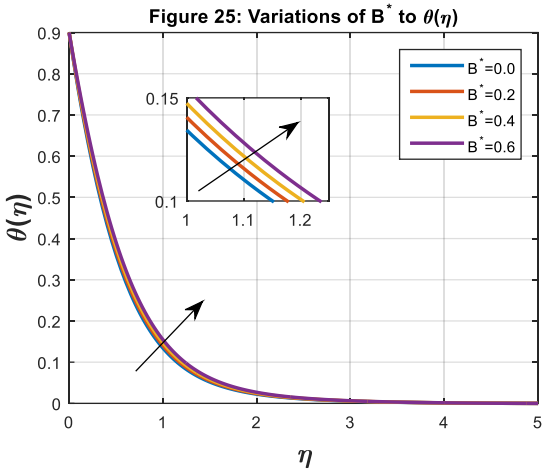

Figure 24 and 25 gives the influence of varying heat source/sink parameters on the temperature distribution θ(η). The results show that an increase in the values A^* and B^* leads to a rise in fluid temperature. Increasing the irregular heat source/sink parameters generates more heat within the flow. The higher fluid temperatures are associated with the values of A^* and B^*.

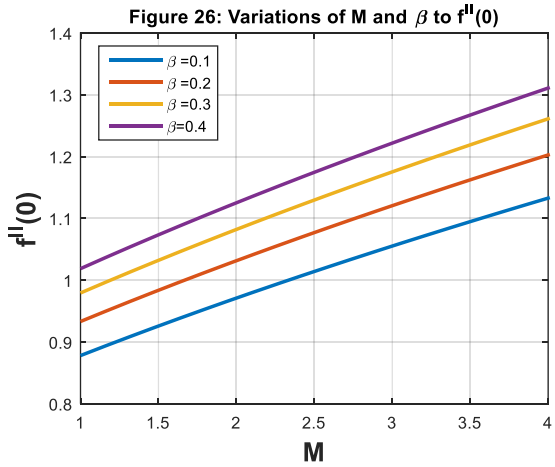

Figure 26 illustrates the inspiration of various strictures, namely M and β, on the drag force factor, denoted as $f''(0)$. The statement indicates that as the values of β and M upsurge, the drag force factor upsurges.

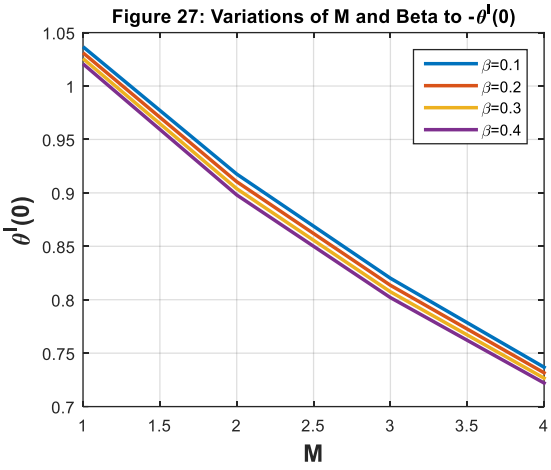

Figure 27 illustrates the inspiration of various strictures, namely M and β, Nusselt number, denoted as $-\theta'(0)$. The statement indicates that as the values of β and M upsurge, the Nusselt Number declines. This is because the magnetic field can weaken convection currents by dampening the flow field.

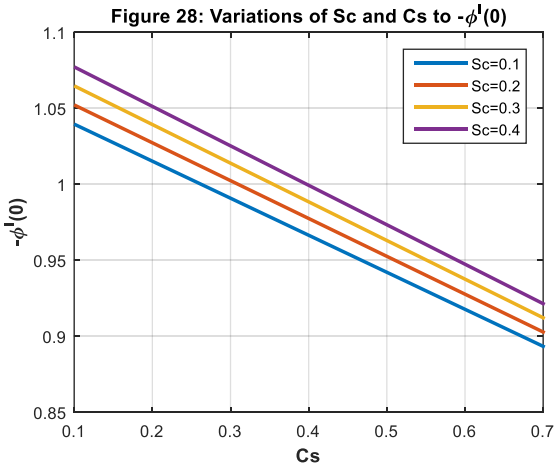

In Figure 28, the variation of the Sherwood number, denoted as $-\phi'(0)$, is demonstrated for (Sc) and the microorganism concentration difference stricture (Cs). The statement indicates that$-\phi'(0)$ is an upsurging function of both Sc and Cs.

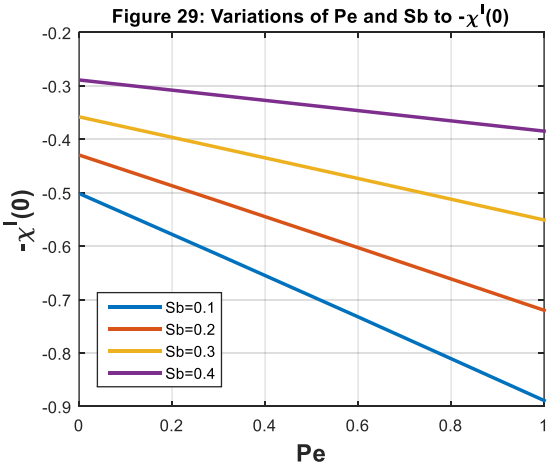

In the figure 29, the variation in the motile microorganism's field, denoted as $-\chi'(0)$, is depicted in response to constraint changes Pe and Sb. The statement indicates that when the values of Pe and Sb increase, there is a corresponding upsurge in the motile microorganism's gradient.

5. Conclusion:

The present work has investigated the bioconvection phenomenon within the Casson nano liquid over an exponentially stretching sheet, considering various parameters, such as magnetic field, nonuniform heat source/sink, activation energy, ohmic dissipation, and motile microorganisms. The governing non-linear ordinary differential equations (ODEs) are solved by using bvp4c. The below are few concluding remarks on the results obtained.

1. The presence of nanoparticles in the Casson fluid enhances thermal conductivity, which significantly impacts the temperature distribution and bioconvection patterns.

2. Higher activation energy influences the temperature gradient and concentration fields, affecting the overall bioconvection process.

3. Motile microorganisms contribute to the bioconvection process by affecting the concentration and velocity fields.

4. The exponential stretching of the sheet introduces non-uniform flow behavior, influencing both velocity and thermal profiles. An increase in the values $A*$ and $B*$ leads to a rise in fluid temperature. Increasing the nonuniform heat source/sink parameters generates more heat within the flow.

References:

[1] Lone, Showkat Ahmad, et al. "A stratified flow of a non-Newtonian Casson fluid comprising microorganisms on a stretching sheet with activation energy." *Scientific Reports* 13.1 (2023): 11240.

[2] Lone, Showkat Ahmad, et al. "Computational analysis of MHD driven bioconvective flow of hybrid Casson nanofluid past a permeable exponential stretching sheet with thermophoresis and Brownian motion effects." *Journal of Magnetism and Magnetic Materials* 580 (2023): 170959.

[3] Jayavel, Prakash, et al. "Homotopy analysis on the bio-inspired radiative magnesium and iron oxides/blood nanofluid flow over an exponential stretching sheet." *Computational Particle Mechanics* 10.6 (2023): 1955-1975.

[4] Mondal, Surya Kanta, and Dulal Pal. "Influence of activation energy and variable thermal conductivity on magneto-convective nonlinear thermo-radiative Casson nanofluid containing motile microorganisms over a sinusoidal surface." *Numerical Heat Transfer, Part A: Applications* (2024): 1-27.

[5] Mandal, Arpita, Hiranmoy Mondal, and Rajat Tripathi. "Activity of motile microorganism in bioconvective nanofluid flow with Arrhenius activation energy." *Journal of Thermal Analysis and Calorimetry* 148.17 (2023): 9113-9130.

[6] Sekhar, M., et al. "Featuring the Stagnation Point Flow of Casson Nanofluid with Thermal Radiation and Swimming Microorganisms over a Stretching Sheet: A Computational Modeling via Analytical Method." *Partial Differential Equations in Applied Mathematics* (2024): 100899.

[7] Shamshuddin, M. D., et al. "Homotopic simulation of MHD bioconvective flow of water-based hybrid nanofluid over a thermal convective exponential stretching surface." *International Journal of Numerical Methods for Heat & Fluid Flow* 34.1 (2024): 31-53.

[8] Waqas, Hassan, et al. "Numerical simulation for bioconvectional flow of burger nanofluid with effects of activation energy and exponential heat source/sink over an inclined wall under the swimming microorganisms." *Scientific Reports* 11.1 (2021): 14305.

[9] Basit, M. A., et al. "Numerical simulation of bioconvective Casson nanofluid through an exponentially permeable stretching surface." *International Journal of Modern Physics B* 38.09 (2024): 2450128.

[10] Ahmad, Iftikhar, et al. "Thermally developed Cattaneo-Christov Maxwell nanofluid over bidirectional periodically accelerated surface with gyrotactic microorganisms and activation energy." *Alexandria Engineering Journal* 59.6 (2020): 4865-4878.
[11] Shamshuddin, M. D., et al. "Bioconvective treatment for the reactive Casson hybrid nanofluid flow past an exponentially stretching sheet with Ohmic heating and mixed convection." *Journal of Thermal Analysis and Calorimetry* 148.21 (2023): 12083-12095.
[12] Makkar, Vinita, Vikas Poply, and Naresh Sharma. "Three Dimensional Modelling of Magnetohydrodynamic Bio-Convective Casson Nanofluid Flow with Buoyancy Effects Over Exponential Stretching Sheet Along with Heat Source & Gyrotactic Micro-Organisms." *Journal of Nanofluids* 12.2 (2023): 535-547.
[13] Khan, Arshad, et al. "Bioconvection Maxwell nanofluid flow over a stretching cylinder influenced by chemically reactive activation energy surrounded by a permeable medium." *Frontiers in Physics* 10 (2023): 1065264.
[14] Imran, Muhammad, et al. "Physical attributes of bio-convection in nanofluid flow through a paraboloid of revolution on horizontal surface with motile microorganisms." *International Communications in Heat and Mass Transfer* 133 (2022): 105947.
[15] Khan, M. Ijaz, et al. "Natural bio-convective flow of Sisko nanofluid subject to gyrotactic microorganisms and activation energy." *Physica Scripta* 94.12 (2019): 125203.
[16] Abdal, Sohaib, et al. "Exploring the magnetohydrodynamic stretched flow of Williamson Maxwell nanofluid through porous matrix over a permeated sheet with bioconvection and activation energy." *Scientific reports* 12.1 (2022): 278.
[17] Siddique, Imran, et al. "Bioconvection of MHD second-grade fluid conveying nanoparticles over an exponentially stretching sheet: A biofuel applications." *Arabian Journal for Science and Engineering* 48.3 (2023): 3367-3380.
[18] Patil, Vishwambhar S., et al. "Analysis of Cattaneo-Christov heat diffusion on MHD Casson-Williamson bioconvective nanofluid flow across an exponential porous stretching sheet." *International Journal of Modelling and Simulation* (2023): 1-20.
[19] Hussain, Zawar, Muhammad Ayaz, and Saeed Islam. "Effects of thermophoresis and Brownian motion on radiative MHD hybrid nanofluid flow over a stretching sheet with convective boundary conditions: A homotopic approach." *Proceedings of the Institution of Mechanical Engineers, Part N: Journal of Nanomaterials, Nanoengineering and Nanosystems* (2024): 23977914231225019.
[20] Habib, Danial, et al. "On the role of bioconvection and activation energy for time dependent nanofluid slip transpiration due to extending domain in the presence of electric and magnetic fields." *Ain Shams Engineering Journal* 13.1 (2022): 101519. (20).
[21] Bafe, Endale Ersino, Mitiku Daba Firdi, and Lemi Guta Enyadene. "Magnetohydrodynamic thermo-bioconvective flow of 3D rotating Williamson nanofluid with Arrhenius activation energy in a Darcy–Forchheimer medium over an exponentially stretching Surface." *International Journal of Thermofluids* 21 (2024): 100585.
[22] Sankari, M. Siva, et al. "Homotopic analysis for bioconvection of Casson nanofluid flow over an exponential stretching sheet with activation energy and motile microorganism." *Numerical Heat Transfer, Part A: Applications* (2024): 1-23.